Machine Learning-Based Surgical State Perception and Collaborative Control for a Vascular Interventional Robot

Yonggan Yan, *Graduate Student Member, IEEE*, Hongbo Wang, *Member, IEEE*, Haoyang Yu, Fuhao Wang, *Graduate Student Member, IEEE*, Junyu Fang, Jianye Niu, and Shuxiang Guo, *Fellow, IEEE*

***Abstract*—In robot-assisted vascular interventional surgery (VIS), surgeons often need to operate outside the operating room to avoid exposure to X-ray. However, it greatly changes the operating ways of surgeons, which affects judgment and operation safety. In this paper, a novel VIS robot system was developed to predict guidewire insertion states and operate collaboratively. To assist the surgeons in perceiving the insertion state, an insertion multi-states prediction model based on softmax logistic regression was proposed. Combined with the prediction model, a human-machine collaborative control strategy was designed, which allows surgeons to perceive the insertion states based on not only the force feedback constructed by the master side but also the prediction results from the slave side. Moreover, a human-machine trust evaluation model and a master-slave collaborative mapping model were proposed for improving safety and efficiency of surgery. To verify the effectiveness of these models, the evaluation experiments in the blood vessel model were carried out. It was indicated by the experiment results that the guidewire insertion states can be predicted by the prediction model in different environments, and the overall accuracy is 93%. The master-slave mapping ratio can be adjusted by the collaborative control strategy automatically to adapt to different surgical conditions. The experimental results showed the usability of the robot-assisted VIS system with the novel force-based perception method.**

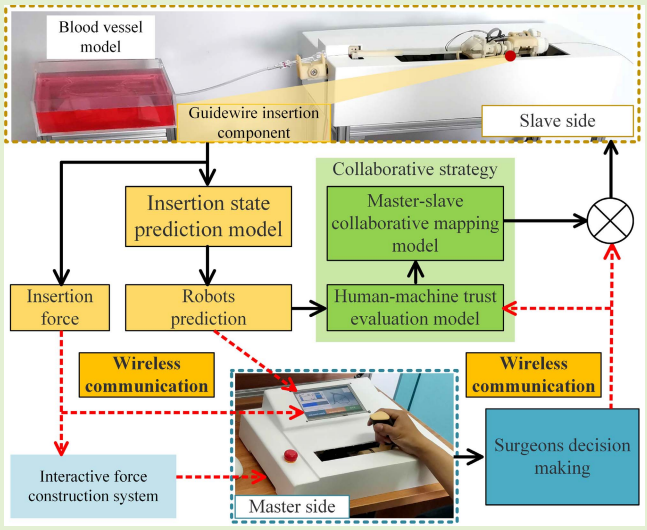

***Index Terms*—Vascular interventional surgery, surgical state perception, human-machine trust, human-machine collaborative control.**

Manuscript received January 26, 2022; accepted February 23, 2022. Date of publication February 25, 2022; date of current version March 31, 2022. This work was supported in part by the National Key Research and Development Program of China under Grant 2019YFB1311700, in part by the National Natural Science Foundation of China under Grant U1713219, and in part by the Shanghai Science and Technology Innovation Action Plan under Grant 18441900700. The associate editor coordinating the review of this article and approving it for publication was Dr. Ravibabu Mulaveesala. *(Corresponding author: Hongbo Wang.)*

Yonggan Yan is with the School of Life Science, Beijing Institute of Technology, Beijing 100081, China, and also with the School of Mechanical Engineering, Yanshan University, Qinhuangdao 066004, China (e-mail: 3120215703@bit.edu.cn).

Hongbo Wang is with the Academy for Engineering and Technology, Fudan University, Shanghai 200433, China, and also with the School of Mechanical Engineering, Yanshan University, Qinhuangdao 066004, China (e-mail: Wanghongbo@fudan.edu.cn).

Haoyang Yu, Junyu Fang, and Jianye Niu are with the Hebei Provincial Key Laboratory of Parallel Robot and Mechatronic System, Yanshan University, Qinhuangdao 066004, China.

Fuhao Wang is with the Academy for Engineering and Technology, Fudan University, Shanghai 200433, China.

Shuxiang Guo is with the Key Laboratory of Convergence Biomedical Engineering System and Healthcare Technology, The Ministry of Industry and Information Technology, Beijing Institute of Technology, Beijing 100081, China.

Digital Object Identifier 10.1109/JSEN.2022.3154921

I. Introduction

CARDIOVASCULAR disease greatly threatens human health and is the biggest killer of humans [1]. Vascular interventional surgery (VIS) has been one of the main methods for the treatment of cardiovascular disease due to small trauma and postoperative recovery [2], [3]. However, the surgery has gradually exposed problems in safety and flexibility [4]–[7], which include the ionizing radiation damage, orthopedic strain injuries caused by surgeons wearing heavy lead-lined radio-protective garments, and the high requirements for the surgical experience. To solve the above problems, the robot-assisted system for VIS has been studied by many companies and research institutions for its advantages of master-slave remote operation, high accuracy, and digitization [8]. The current research mainly focuses on the mechanical structure design of the master-slave VIS robot [8]–[12], the active bending control of interventional medical devices [13], [14], and the collection and application of intraoperative information [7], [15]–[27]. Although substantial achievements have been witnessed in robot-assisted VIS during the past few decades, surgery force

state perception and the human-machine collaborative control remain difficult [28], [29]. Nevertheless, it is theoretically significant and practically valuable to solve the above two problems.

Surgeons mainly insert interventional medical devices by observing the images of the DSA (digital subtraction angiography) system during VIS. Experienced surgeons also perceive the insertion force with their haptic sense for the judgment of the insertion state and the decision making of surgical operations [7]. Unlike surgery in the operating room, surgeons rely on the interactive force with the master manipulator to feel the insertion force of interventional medical devices. Therefore, it is valuable to achieve the remote force state perception. Many studies focus on the establishment of the master manipulator interactive force and achieve remarkable results [7], [15]–[20]. However, almost all master manipulator control methods are different from the actual interventional medical devices. Some master-slave systems use commercial operators directly [11], [21]–[23], but the DOFs (degrees of freedom) and shape of these operating handles are different from the catheter and guidewire. Other parts consider the surgeons' habitual operating mode of manipulating a catheter and design the catheter-based master manipulators [7], [24]–[26], but the manipulation inertia is different due to the fixed connection of various components of the catheter. Therefore, the above two force feedback methods are limited in helping surgeons to judge the surgical state.

The slave manipulator can measure surgical signals of devices in real time and digitally without data transmitting over systems. Therefore, it is a reasonable way to predict the surgical state intelligently based on the force and position data collected by the slave side during operating. In that case, robots can do two tasks during surgeons using robots for VIS. On the one hand, the master manipulator creates interactive force with the surgeons based on the slave side data, which can be reduced requirements in the natural sense to an extent. On the other hand, the slave manipulator predicts the state of interventional devices based on the surgical signals and provides the results to the human-machine interface (HMI) in real time to assist surgeons in decision making. To improve the safety and efficiency of surgery, the human-machine collaborative state can be evaluated based on the robot prediction results and the surgeons' decisions. The human-machine manipulation parameters can be adjusted by the evaluated state to adapt to different surgical conditions.

Machine learning is an important method for computers to achieve human-like learning capabilities and has been used in VIS robots. Guo *et al.* [22] modeled unstructured surgeons' surgical skills based on convolutional neural networks (CNN) and realized the navigation of guidewire in the simple blood vessel model. They also evaluated surgical operation skills based on machine learning for improving the surgical outcome and robots performance [23]. Chi *et al.* [27] proposed a method combining non-rigid registration and Gaussian mixture model (GMM) and applied it to similar models for autonomous robot intervention. However, the above image-based surgical state prediction methods are limited in the small and complex coronary arteries or renal arteries. Under these conditions, the force-based methods often perform better in state prediction and safety.

Some studies achieved safety protection in emergencies by setting the insertion force threshold [16], [18]. However, on the premise of ensuring the completion of insertion operations and safe contact force with blood vessels, setting the force threshold size in different environments is also a difficulty. At present, there are few results on the prediction of multiple insertion states of the guidewire based on the operation force and position signals.

To this end, this paper sets out to propose a human-machine collaborative control strategy for a VIS robot and a guidewire insertion multi-states prediction model based on softmax logistic regression. To collect the guidewire insertion force and construct interaction force for surgeons, a guidewire insertion force extraction model and a human-machine interaction force construction system are designed. Based on the prediction model, a human-machine trust evaluation model and a master-slave collaborative mapping model are proposed for improving the safety and efficiency of surgery. A force and position collection platform was built for collecting data sets of the left anterior descending branch (LAD) and left circumflex branch (LCX) of the coronary artery. Finally, a human-machine collaborative surgery platform was built to test the accuracy of the force-based prediction model and the feasibility of the collaborative control strategy.

The remainder of this paper is organized as follows. Section II introduces the proposed collaborative control strategy, the VIS robot system, and the detail of the control algorithms. In section III, evaluation experiments are presented to verify the accuracy and performance of the robot system and the proposed models. Section IV is the discussion. Finally, the conclusion is given in Section V.

II. Methodology

A. Human-Machine Collaborative Control Strategy

Ionizing radiation harms surgeons during surgery, so the VIS robot based on master-slave remote control strategy has become a promising direction. The basic architecture is composed of a master manipulator, a slave manipulator, and remote communication equipment [30]. When surgeons operate remotely, the real-time and effective feedback of data determines the quality and safety of the operation. However, the difference between the master manipulator and the interventional devices and the delay, which is caused by the wireless communication and the transmitting of each acquisition system, greatly affect the surgeons' judgment. Then it reduces the safety of surgery with VIS robot.

To assist surgeons in predicting surgical state and decrease the requirements of accuracy and real time ability in force feedback, a human-machine collaborative control strategy is proposed as shown in Fig. 1. Unlike the existing control strategies in other VIS robots [19], [20], the strategy allows surgeons to perceive the operation state based on not only the force feedback constructed by the

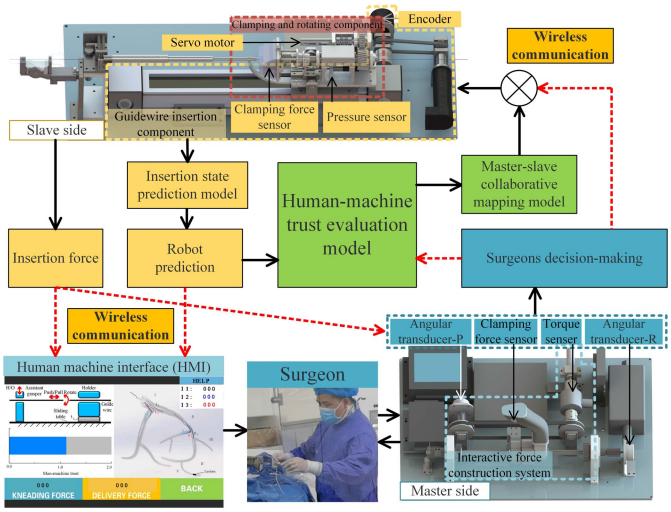

Fig. 1. Human–machine collaborative control strategy.

master side but also the prediction results from the slave side.

The surgeons judge the surgical state by observing the operation information through the HMI and feeling the interactive force created by the master manipulator. The master manipulator collects the surgeons' operation data through the torque sensor (JNNT-S-1Nm, BENGBU SENSOR, China), clamping force sensor (FlexiForce 1lbsA201, TEKSCAN, US), angular transducer-P (P2500, MIRAN, China), and angular transducer-R (P2500, MIRAN, China). And it transmits the data to the slave manipulator wirelessly in real time, which is the input of the multi-closed-loop system on the slave side. The slave manipulator clamps, rotates, and inserts the guidewire under closed-loop control. The insertion force sensor (SBT674-19.6N, SIMBATOUCH, China) and the encoder (RW-ARE-485-RTU-11-5-m-6, REALWETECH, China) of the slave side collect the current insertion force and position data. Then based on the insertion state prediction model, the slave side predicts the insertion states of the guidewire intelligently in the blood vessel. Besides, the prediction results and the insertion force data are fed back to the HMI and interaction force construction system wirelessly to assist the surgeons. So far, the master-slave system for VIS completes a period operation. To show the effect of the robot prediction on surgery, the human-machine collaborative operation performance is evaluated by the human-machine trust evaluation model based on the human-machine operation results. And it can adapt to different surgical conditions by adjusting the master-slave mapping ratio to improve the safety and efficiency of surgeons using robots for VIS.

B. Human-Machine Interaction Force Construction

The slave manipulator is shown in Fig. 2(a). It is a reciprocating push/pull guidewire operation structure, which mainly includes the insertion component, the clamping and rotating component, the telescopic rod component, and a micro controller unit (MCU). It can insert, clamp, rotate the guidewire, and measure the insertion force and position. To improve the measurement ability of weak insertion force, the force measuring mechanism was designed based on the principle of moment balance as shown in Fig. 2(b). It is a simple lever to amplify the insertion force. The upper platform is connected with the lower platform through a hinge, and the latter is installed with a pressure sensor for measuring the pressure perpendicular to its plane. The insertion force along the axis of the clamping jaw is amplified by 3.5 times based on the principle of moment balance and measured by the pressure sensor. This structure enhances the ability to measure weak force signals, and the overall accuracy reaches 5.6mN. However, the force data includes the insertion force and the inertial force of the mechanism. Furthermore, the former is weaker than the latter, so an insertion force extraction model was designed. The schematic diagram of the insertion force measuring mechanism is shown in Fig. 2(c). From the diagram, the insertion force in this state is expressed as the follow equations:

$$f = \frac{Fs - [\sum_{i=1}^{k}(m_i r_i g + m_i h_i a_1) + (m_1 h_b + m_2 h_a)a_2]}{h_s} \quad (1)$$

where f represents the guidewire insertion force, F represents the force of the pressure sensor, s represents the horizontal distance between the force measuring point and the hinge axis, m_i represents the mass of the i-th part, m_1 represents the mass of the screw nut, m_2 represents the mass of the connection plate, r_i represents the horizontal distance between the center of gravity of the i-th part and the axis of the hinge axis, h_i represents the vertical distance between the center of gravity of the i-th part and the hinge axis, h_1 represents the vertical distance between the center of gravity of the screw nut and the hinge axis, h_2 represents the vertical distance between the center of gravity of the connection plate and the hinge axis, h_s represents the vertical distance between the guidewire axis and the hinge axis, a_1 represents the guidewire clamping and rotating component acceleration, a_2 represents the acceleration of the screw nut and connection plate, g represents the acceleration of gravity, k represents the total number of parts.

The master manipulator is shown in Fig. 3. Same as the slave side, it was designed with three DOFs: push/pull, rotating, and clamping. It is mainly composed of the interaction force construction system, angular transducer-P, angular transducer-R, several signal transmitters, and an MCU. The master manipulator position signal of the push/pull motion is collected by the angular transducer-P at one end of the synchronous belt. And the other end of the synchronous belt is driven by a servo motor (RE13, Maxon, Switzerland). A torque sensor is installed between the servo motor and synchronous belt to measure the human-machine interaction force. On the one hand, the interactive force signal is filtered to predict the surgeons' operation intention and drive the servo motor. It can reduce the resistance during operation. On the other hand, a force closed-loop was formed to realize the surgeons' perception of the remote insertion force extracted from the slave side. The position signal of the rotating motion

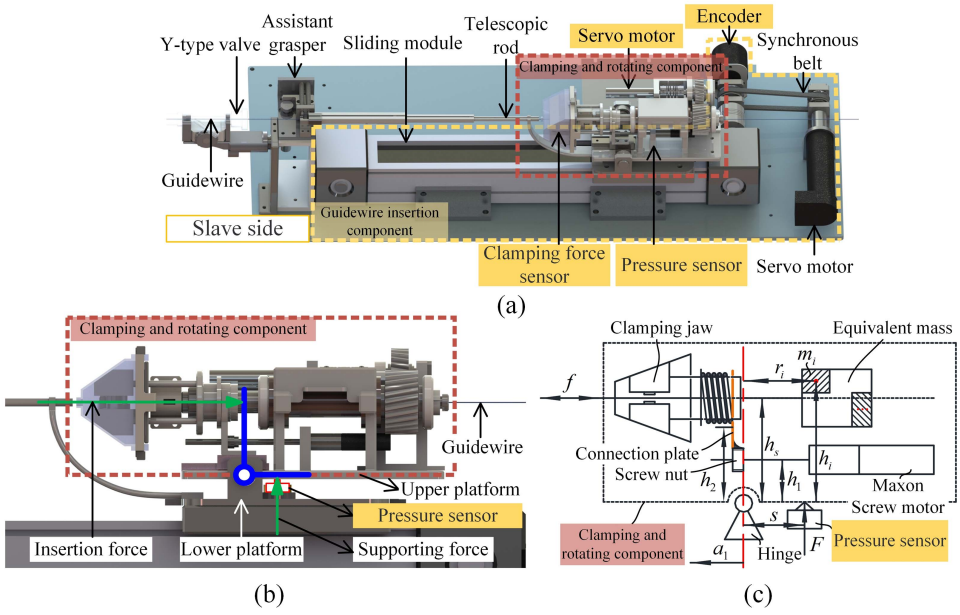

Fig. 2. The slave manipulator. (a) Schematic structure. (b) Insertion force measuring mechanism. (c) The schematic diagram of the measuring mechanism.

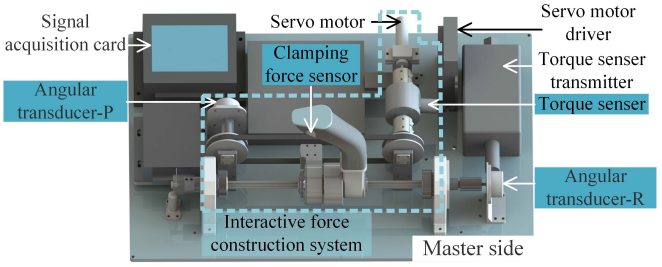

Fig. 3. The master manipulator.

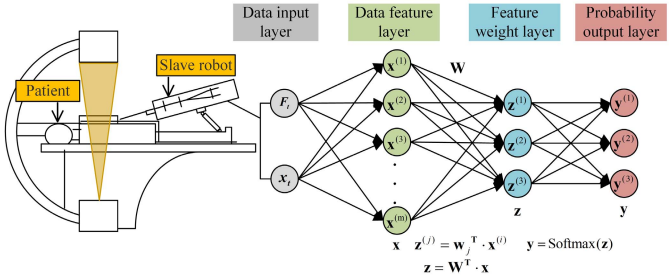

Fig. 4. The guidewire insertion multi-states prediction model. Where $\boldsymbol{F_t}$ represents the original data matrix of the guidewire insertion force, x_t represents the absolute depth data matrix of insertion, $\mathbf{x^{(i)}}$ represents the feature matrix of the *i*-th experimental sample, x the total feature matrix of all experimental sample, w_j^T represents the feature weight of the label *j*, W^T represents the total feature weight matrix, $z^{(j)}$ represents the dot product of the feature matrix and the weight matrix of the label *j*, z represents the dot product of the total feature matrix and the total weight matrix, $y^{(j)}$ represents the predicted probability matrix of the label *j*, y represents the probability prediction matrix of all categories, Softmax(·) represents softmax logistic regression model.

is collected by the angular transducer-R coaxial link with the handle.

C. Guidewire Insertion State Prediction Model

Human blood vessels are winding and complex, especially in the coronary artery. The guidewire insertion force is related to many factors during operation, which mainly includes the shape of blood vessels, the depth of insertion, and the number of bifurcations. The insertion resistance of guidewire in blood vessels mainly includes blood viscous resistance, the friction between the guidewire and the blood vessel wall, and the resistance caused by the guidewire tip piercing the blood vessel wall. The size of the insertion force increases gradually with the depth of insertion, especially at the large curvature of the blood vessels and the bifurcations. Therefore, the effect of simply setting the threshold of the insertion force to predict insertion state or ensure safe insertion is limited. Yan *et al.* [22] proposed a 1D CNN-based method, which can predict the unstructured surgical abnormal states. It performs the feasibility of the force-based prediction method. However, the model can only predict whether the current operating force state is abnormal for safety. Nevertheless, more detailed states of insertion are vital for surgeons without real perception. Therefore, we proposed an insertion multi-states perception model for solving the problem.

After planning the vascular intervention path, the distal end of the guidewire was mainly divided into three states during the insertion: passing the bifurcation, entering the bifurcation, and obstructed. To predict the states, a guidewire insertion multi-states prediction model based on machine learning was proposed. The prediction function was completed in an MCU with limited computing power to avoid communication delays-between devices. Therefore, a low computational algorithm that can achieve multi-classification, namely the softmax logical regression, was considered in this paper. It considered the features of the insertion position and the trend of the insertion force with the position. The state prediction model is shown in Fig. 4.

For the i-th training sample, the probability prediction model belonging to the label j is expressed as the follow equations:

$$P\{\mathrm{y}^{(i)} = j|\mathrm{x}^{(i)};\theta\} = \frac{e^{\theta_j{}^{\mathrm{T}}\mathrm{x}^{(i)}}}{\sum_{l=1}^{3} e^{\theta_l{}^{\mathrm{T}}\mathrm{x}^{(i)}}} \tag{2}$$

where $j \in \{0, 1, 2\}$ represents passing by the bifurcation, entering the bifurcation, and obstructed, respectively, θ represents the weight matrix.

The cost function is shown as (3). The model was trained using batch gradient descent. The regularizing term was added to the cost function to reduce the overfitting caused by the small sample size. The gradient expression is shown as (4):

$$J_\theta = -\frac{1}{m}\left[\sum_{i=1}^{m}\sum_{j=1}^{3} I\{\mathrm{y}^{(i)}{=}j\} \ln \frac{e^{\theta_j{}^{\mathrm{T}}\mathrm{x}^{(i)}}}{\sum_{l=1}^{3} e^{\theta_l{}^{\mathrm{T}}\mathrm{x}^{(i)}}}\right] + \lambda\sum_{i=1}^{3}\sum_{j=1}^{n}\theta_{ij}{}^2 \tag{3}$$

$$\nabla_{\theta_j} J_\theta = -\frac{1}{m}\left[\sum_{i=1}^{m} \mathrm{x}^{(i)}(I\{\mathrm{y}^{(i)} = j\} - P\{\mathrm{y}^{(i)} = j|\mathrm{x}^{(i)};\theta\})\right] + \lambda\theta_j \tag{4}$$

where J_θ represents the cost function, λ represents the regularization parameter, m represents the number of samples, $I\{\cdot\}$ represents the indicator function.

D. Human-Machine Trust Evaluation Model

In the human-machine system, Moray *et al.* [31] proposed that human trust in robots mainly depends on three factors: robot performance, human performance, and environmental factors. Among them, the human-machine trust is closely related to robot performance and moderately related to human performance and environmental factors. It is vital for the working and efficiency of system. Zhao [32] proposed a human-machine trust evaluation model. The model can set the probability threshold based on the probability of the operating abnormal force and dynamically adjust the master-slave mapping ratio to improve safety. However, on the one hand, the trust evaluation model only evaluates the performance of the robot. The operating information of surgeons, which includes much implicit information, is also essential for the trust evaluation. On the other hand, the operating force mode recognizer can only predict whether the operation is abnormal or not, without considering the human-machine operation results under normal states.

To evaluate the operator and robot operation, we designed the robot performance evaluation model and the operator's. Further, based on the performance evaluation models, a trust evaluation model was designed to evaluate the agreement degree of human-machine decision making and characterize the current device insertion environment. As the application of the trust evaluation model, the master-slave mapping ratio is adjusted to adapt to the different operation states. It can not only perform micro-operations to improve the safety and operation accuracy when the human-machine trust is low but also insert the guidewire rapidly to improve the efficiency of the operation when the trust is high.

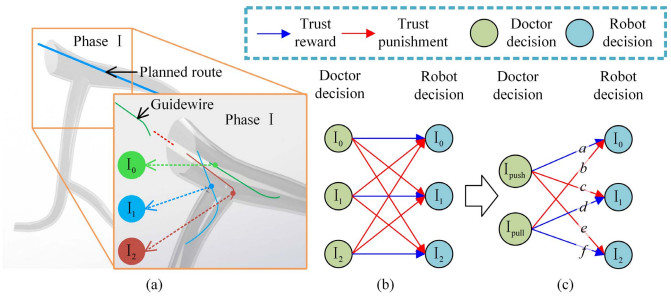

Fig. 5. The human–machine decision making state analysis diagram. (a) Three possible states in phase I. (b) Human-machine decision making results. (c) Converted decision making results.

1) Surgeons Operation Performance Evaluation Model: As shown in Fig. 5(a), the planned route of the guidewire in the phase I is passing by the bifurcation. The insertion has three possible states: I_0, I_1, and I_2, and they represent passing by the bifurcation, entering the bifurcation, and obstructed, respectively. As shown in Fig. 5(b), the human-machine decision making results have 9 states. The blue arrows indicate that the results are consistent, and the red arrows indicate that the results are inconsistent. The surgeons' judgments are often implicit thinking. To collect and recognize it, the 9 states are converted into 6 states as shown in Fig. 5(c). Where I_{push} represents pushing the guidewire, I_{pull} represents pulling the guidewire. On the one hand, the surgeons' operation speed is positively correlated with the confidence of the operation, that is, the higher the operation speed, the more certain the operation. On the other hand, compared with the last collection window, the change of the current speed also reflects the surgeons' confidence in the current prediction. When the dynamic speed increases, it means that the surgeons' confidence in the current state is increasing. On the contrary, when the dynamic speed decreases, it means that the current surgeons' confidence is less than the last collection time. Combined with the dynamic speed, the trust evaluation model can avoid the condition that the surgeons' operating speed decreases sharply, but the human-machine trust is still increasing. The sign of the surgeons' operating performance is determined by pushing or pulling operation. So the surgeons' operating performance can be preliminarily expressed by:

$$P_{\mathrm{H}}(t) = \mathrm{sgn}(\Delta x(t)) \cdot |\Delta\dot{x}(t)| \cdot \frac{|\Delta\dot{x}(t)|}{|\Delta\dot{x}(t-1)| + |\Delta\dot{x}(t)|} \tag{5}$$

where $P_{\mathrm{H}}(t)$ represents the surgeons' operation performance, $P_{\mathrm{H}}(t) \in [-1, 1]$, $\Delta x(t)$ represents the operating displacement at time t, signum function $\mathrm{sgn}(\Delta x(t)) = \begin{cases} 1, & \Delta x(t) \geq 0 \\ -1, & \Delta x(t) < 0 \end{cases}$, $|\Delta\dot{x}(t)|$ represents the operating speed at time t, $|\Delta\dot{x}(t-1)|$ represents the operating speed at time $t-1$.

Normalize the expressions in (5) except for the signum function, as shown in (6). Normalization can adjust the performance of operator to the range of [0, 1) and ensure sensitivity

TABLE I
POSSIBLE CONDITIONS IN PHASE I

State	Surgeons decision	Maximum probability label of prediction
a	$\mathrm{I}_{\mathrm{push}}$	I_0
b	$\mathrm{I}_{\mathrm{pull}}$	I_0
c	$\mathrm{I}_{\mathrm{push}}$	I_1
d	$\mathrm{I}_{\mathrm{pull}}$	I_1
e	$\mathrm{I}_{\mathrm{push}}$	I_2
f	$\mathrm{I}_{\mathrm{pull}}$	I_2

TABLE II
ROBOT PERFORMANCE IN VARIOUS OPERATING STATES

Operator performance $P_{\mathrm{H}}(t)$	Robot prediction state	Robot performance $\lvert P_{\mathrm{R}}(t)\rvert$	Human-machine decision results
$P_{\mathrm{H}}(t) \geq 0$	I_0	$P_{\mathrm{E}}(t)$	Same
	I_1, I_2	$1 - P_{\mathrm{E}}(t)$	Difference
$P_{\mathrm{H}}(t) < 0$	I_0	$P_{\mathrm{E}}(t)$	Difference
	I_1, I_2	$1 - P_{\mathrm{E}}(t)$	Same

Where $P_{\mathrm{E}}(t)$ represents the predicted probability of the desired label at time t. For example, in the phase I $P_{\mathrm{E}}(t)$=$P_0(t)$.

during low-speed operation.

$$P_{\mathrm{H}}(t) = \mathrm{sgn}(\Delta x(t)) \cdot \frac{2}{\pi} \cdot \mathrm{atan}(|\Delta \dot{x}(t)| \cdot \frac{|\Delta \dot{x}(t)|}{|\Delta \dot{x}(t-1)| + |\Delta \dot{x}(t)|}) \tag{6}$$

2) Robot Performance Evaluation Model: The performance of the robot is mainly determined by the prediction results of the robot, which is expressed as:

$$P_{\mathrm{r}}(t) = \left[P_0(t) \;\; P_1(t) \;\; P_2(t) \right] \tag{7}$$

where $P_{\mathrm{r}}(t)$ represents the predicted probability matrix of the guidewire insertion state at time t, $P_j(t)$ represents the predicted probability of the insertion state label j at time t.

As shown in Fig. 5(c) and TABLE I, there are 6 human-machine decision making results from a to f in the phase I. In the states of a and b, the predicted probability of label I_0 is the largest, and the label is the desired state. The state of a is interpreted as the surgeons agreeing with the current prediction results and continuing inserting. The state of b is interpreted as the surgeons disagreeing with the results and withdrawing the guidewire for the next attempt. Similarly, the states of c and e are interpreted as the surgeons disagreeing with the current prediction results and considering the current state as the desired state. The states of d and f are interpreted as the surgeons agreeing with the current prediction of the undesired insertion state and withdrawing the guidewire. The robot performance in various operating states can be summarized as shown in TABLE II.

It can be concluded from TABLE II that when the robot prediction result is consistent with the desired state, that is, $\max(P_{\mathrm{r}}(t)) = P_{\mathrm{E}}(t)$, the robot performance degree is characterized as $P_E(t)$. When $\max(P_{\mathrm{r}}(t)) \neq P_{\mathrm{E}}(t)$, the robot performance degree is characterized as $1 - P_{\mathrm{E}}(t)$. Further, combined with the human-machine decision results, the rule is expressed as:

$$P_{\mathrm{R}}(t) = \mathrm{sgn}(P_{\mathrm{H}}(t)) \cdot (P_{\mathrm{E}}(t) - I(\max(P_{\mathrm{r}}(t)) \neq P_{\mathrm{E}}(t))) \tag{8}$$

where $P_{\mathrm{R}}(t)$ represents the robot performance, $P_{\mathrm{R}}(t) \in [-1, 1]$,

$$I(\max(P_{\mathrm{r}}(t)) \neq P_{\mathrm{E}}(t)) = \begin{cases} 0, & \max(P_{\mathrm{r}}(t)) = P_{\mathrm{E}}(t) \\ 1, & \max(P_{\mathrm{r}}(t)) \neq P_{\mathrm{E}}(t) \end{cases}.$$

3) Human-Machine Trust Model: At time $t = 0$, the human-machine trust $T(0) = 1$, then $T(t)$ is rewarded or punished based on $T(t-1)$. The human-machine trust evaluation model is expressed as:

$$T(t) = T(t-1) + |P_{\mathrm{H}}(t)| \cdot P_{\mathrm{R}}(t) + E(t) \tag{9}$$

where $T(t)$ represents the human-machine trust at time t, $T(t) \in [0, 2]$, $E(t)$ is set as a parameter related to the number of undesired operations. The number of undesired operations within a certain range of motion characterizes the complexity of the current environment to an extent. $E(t)$ is simply expressed as:

$$E(t) = -0.5 \times \sum_{p=1}^{3} Wd_p \tag{10}$$

where Wd_p represents the number of withdrawing at phase p.

E. Master-Slave Collaborative Mapping Model

Predictably, the robot prediction has a certain error rate due to the complex artery environment and incomplete data set. Therefore, on the premise of not changing the results of the surgeons' decision making, the human-machine trust model is only used to adjust the master-slave mapping ratio dynamically.

The master-salve mapping ratio was set to three modes: micro-operation, unit mapping operation, and efficient operation. The micro-operation mode, in which the human-machine trust is in the range of 0 to 0.5, is switched to improve the safety of the operation by decreasing the master-slave mapping ratio. It shows that the current guidewire insertion environment is complex and the human-machine collaboration degree is low. The unit mapping operation mode, in which the trust is in the range of 0.5 to 1.5, is the default operation mode. When the trust is in the range of 1.5 to 2, the system switches to the efficient operation mode. It is considered that the insertion environment is simple and the collaboration degree is high. This mode improves the operation efficiency by increasing the master-slave mapping ratio.

To avoid the decrease of the robot system robustness due to the frequent switching of the boundary between the three modes, the hyperbolic tangent function was used to smooth boundaries, and the master-slave mapping model is shown in (11) and Fig. 6.

$$k(T(t)) = \begin{cases} 0.25 \tanh(T(t) - 0.5) + 0.75 & T(t) \in [0, 1] \\ 0.25 \tanh(T(t) - 1.5) + 1.25 & T(t) \in (1, 2] \end{cases} \tag{11}$$

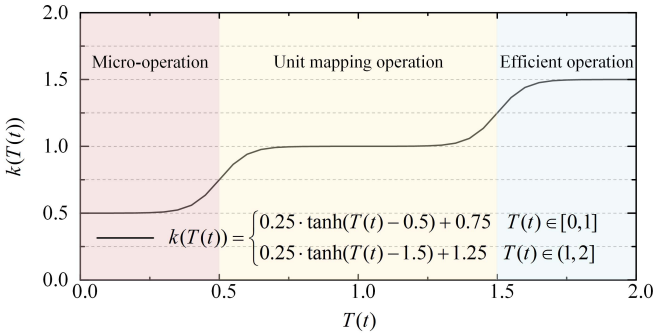

Fig. 6. Three operation modes and master-slave mapping curve.

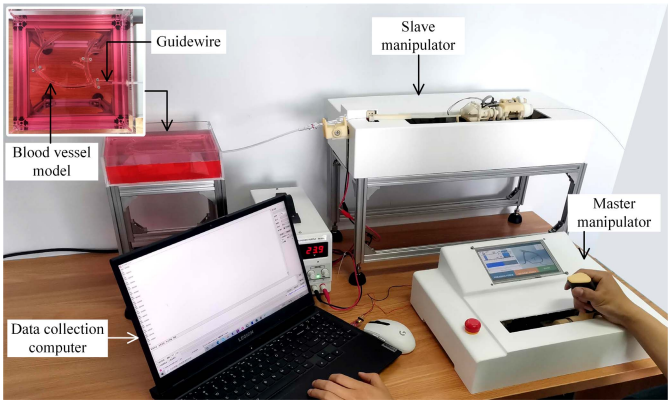

Fig. 7. Data collection platform.

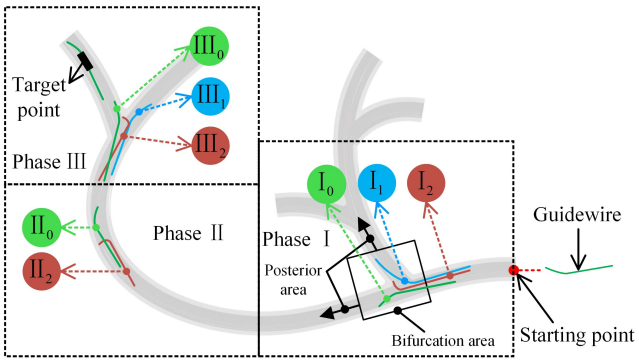

Fig. 8. Data collection platform.

F. Hardware Setup and Data Collection

To collect data for model training, a data collection platform was built, as shown in Fig. 7. It mainly includes the master manipulator, the slave manipulator, a blood vessel model, and a data collection computer. The blood vessel model is an equal inner diameter resin model resembling the LAD and LCX of the coronary artery, as shown in Fig. 8.

A target point was marked at the blood vessel model bifurcation. The guidewire needs to pass two bifurcations during the insertion process. According to the bifurcation and curvature at different positions, the blood vessel model was divided into phase I, phase II, and phase III. Each phase contains features that affect the insertion state.

In the phase I, when the rotating angle of the guidewire with the head bend is right, the guidewire will pass by the bifurcation smoothly as shown by the green guidewire I_0 in Fig. 8. In this state, the guidewire contacts with the inner wall of the blood vessel smoothly, and the insertion force hardly increases with the insertion depth; When the guidewire enters the bifurcation as shown by the blue guidewire state I_1. The contact with the inner wall of the blood vessel is also smooth, but the insertion force will increase slightly with the insertion depth; When the guidewire is obstructed as shown in the red guidewire state I_2. The guidewire has a larger contact force with the inner wall of the blood vessel model, and the insertion force will increase greatly with depth. The phase III is similar to the phase I, but the insertion force is different due to the different absolute position and the bifurcation shape. In the phase II, the blood vessel model has no bifurcation, but the curvature of the model is notable and the insertion force also increases to a certain extent.

As shown in Fig. 8, the starting point and the target point were set on the blood vessel model, and data were collected in the phases I, II, and III, respectively. The VIS robot was controlled to insert within the range of the current phase repeatedly with the rotated guidewire randomly. The labels, insertion force, and position data were collected in real time, and 1800 sets of data and labels were collected to form the original data sets of the three phases.

Eight features were extracted to form the sample feature matrix: standard deviation, maximum insertion force, insertion force range, overall linear regression, average force and linear regression in the bifurcation area, and average force and linear regression in the posterior area. The label matrix was composed of the training sample labels of each phase, which were converted to one-hot encoding. The data set of each phase was divided into 10 samples by stratified random sampling, in which the test set was 30% and the training set was 70%. Then the divided data set was standardized. The training data set was formed with the feature matrix with the bias term and the label matrix. The training model was optimized by the batch gradient descent method. The learning rate was initially set as 0.05. After training, the optimized model was obtained.

III. Evaluation Experiments and Results

A. Performance Evaluation of Master-Slave Displacement Tracking

Master-slave displacement tracking performance is a vital parameter for evaluating the VIS robot. In the experiment, the operator's operation displacement was measured by the angular transducer-P of the master side, and the tracking displacement of the slave manipulator was measured by an 11-bit encoder. The wireless module (NRF24L01, HOLYIOT, China) was used to realize the master-slave remote communication and construct the master-slave remote displacement closed-loop. The master-slave mapping ratio was set to 1, and the operator pushed and pulled 8 times at different speeds, which were marked as tests A to H. The measured master-slave

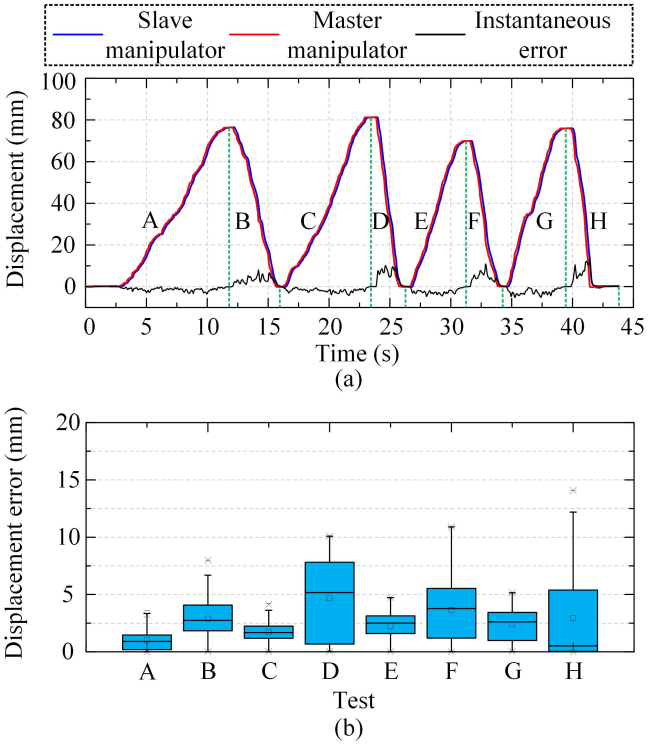

Fig. 9. Experimental results for displacement tracking. (a) Displacement tracking curve. (b) Tracking error boxplot.

displacement tracking curve and the error boxplot are shown in Fig. 9.

The average dynamic tracking error was 2.228787 mm, and the average relative dynamic tracking error was 2.74%, which met the requirement for surgeons to operate guidewire accuracy. In tests B, D, F, and H, the tracking error was relatively large due to the existence of the master-slave teleoperation delay and the relatively high operating speed. In test H, the average speed was 47.47 mm/s, the maximum instantaneous speed was 126.07 mm/s, the maximum dynamic tracking error was 14.08 mm, and the maximum relative dynamic tracking error was 17.33%. From Fig. 9(b), the slower operation, the lower the maximum tracking error, and the lower the median error. In other words, lowering the operation or decreasing the master-slave mapping rate is an effective method to improve the operation accuracy.

B. Performance Evaluation of Master-Slave Insertion Force Feedback

In this section, two experiments were performed to verify (1) and evaluate the performance of the master-slave force feedback. The experimental setup is shown in Fig. 10. It includes the insertion force measuring component of the slave side and the interaction force construction system of the master side.

The theoretical equivalent mass is 1.11 kg by substituting the models' parameters into (1). The mass can be verified by measuring the pressure under the uniform acceleration motion of the slave robot. In the inertial force verification experiment, the acceleration was set to 18mm/s^2, and the position and force

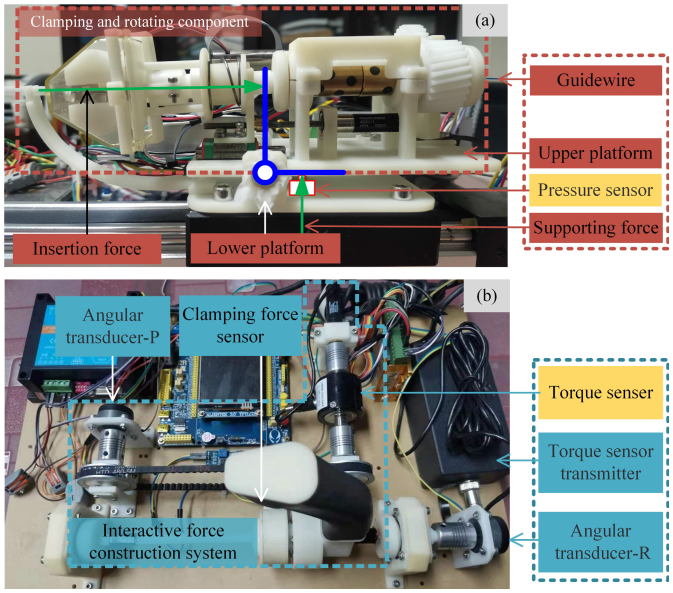

Fig. 10. Experimental setup for force feedback evaluation. (a) Guidewire insertion force measuring component of slave side. (b) Interaction force construction system of master side.

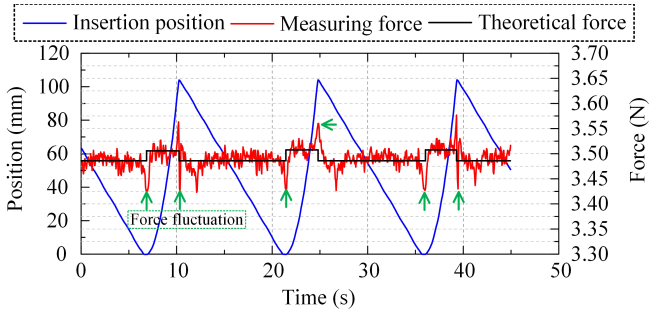

Fig. 11. Results of inertial force verification experiment.

data were measured by the encoder and the pressure sensor, respectively, as shown in Fig. 2(a). The results of the inertial force verification experiment are shown in Fig. 11, where the blue line represents the insertion displacement, the red line represents the measuring force, and the black line represents the theoretical force under (1). The results suggested that the theoretical mass conformed to the measurement results, so it can replace the actual inertia. The green arrows, shown in Fig. 11, are large fluctuations in the measuring force at the beginning and end of acceleration. The reasons are the flexible impact caused by the sudden uniform acceleration movement and the rigid impact at the endpoint. In other cases, we dealt with this problem.

In the performance evaluation experiment of force feedback, the torque sensor of the master side and the pressure sensor of the slave side were used to collect the human-machine interaction force and the guidewire insertion force in real time, respectively. The communication between the master and the slave was realized by the wireless module, and a master-slave operation force closed-loop system was constructed. To make the operator feel the feedback force clearly, the master-slave force mapping ratio was set to 6:1 initially. When

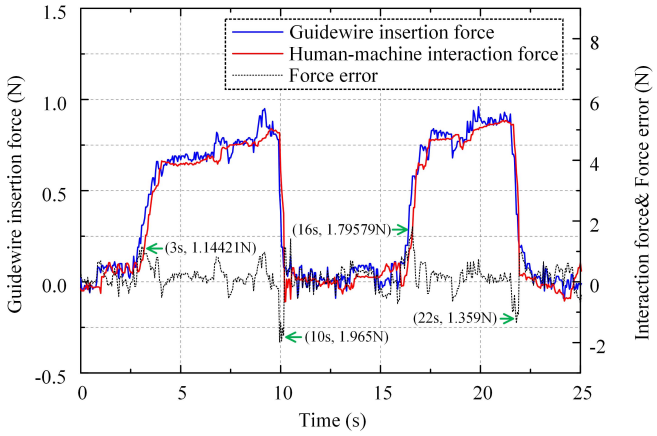

Fig. 12. Experimental results of the master–slave insertion force feedback.

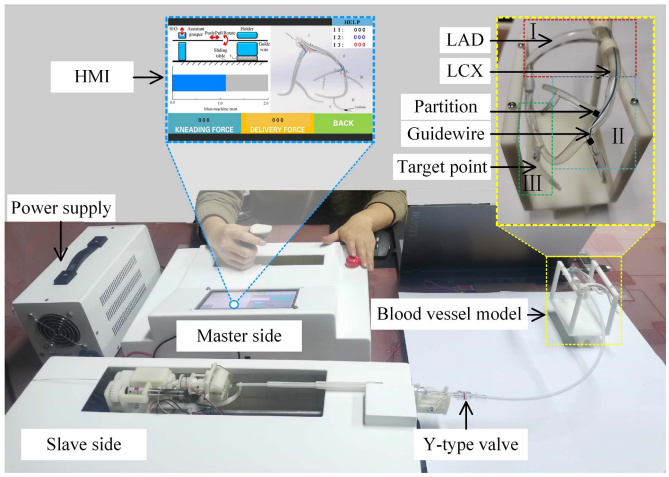

Fig. 13. Experimental setup for the performance evaluation of the prediction model and the collaborative strategy.

the operator manipulated the master side, a guidewire insertion resistance was applied at the slave side actively. As the input of the interactive force construction system, the resistance was extracted by the slave side and transmitted to the master side. Then the input force was amplified 6 times by the master side for the operator. The experimental results of the master-slave insertion force feedback are shown in Fig. 12. The average dynamic error was 0.338 N, and the average relative dynamic error was 6.37%. At about 3 s, 10 s, 16 s, and 22 s, the dynamic errors were 1.14421 N, 1.965 N, 1.79579 N, and 1.359 N, respectively. The guidewire insertion resistance at the above moments has large fluctuations. The reasons are the system delay and the amplification of the mapping ratio. The force error was also amplified 6 times. Besides, the force feedback accuracy requirement can be reduced to an extent when the guidewire insertion prediction model works.

C. Performance Evaluation of the Guidewire Insertion Prediction Model

The experimental setup for the performance evaluation of the prediction model is shown in Fig. 13, which mainly includes the master manipulator, the slave manipulator, and the blood vessel model. The model includes the LAD and LCX, which was divided into three phases: I, II, III, similarly. The target point was set at the end branch of the LCX. The operator observed the current surgical information in the HMI and manipulated the master side to insert the guidewire. During the process, the slave side collected the force and position signals in real time, and the insertion states were predicted by the optimized prediction model.

In the evaluation experiment of the prediction model, the operator repeatedly inserted the guidewire 100 times. The angle of the guidewire was rotated randomly for each operation. The label with the largest probability among the three labels was set as the final prediction result. The actual results and the prediction results of the 100 operations are shown in Fig. 14. Among 100 prediction results, 2, 3, and 2 prediction errors existed in label 2, label 1, and label 0, respectively. The prediction accuracy of the insertion state was 93%.

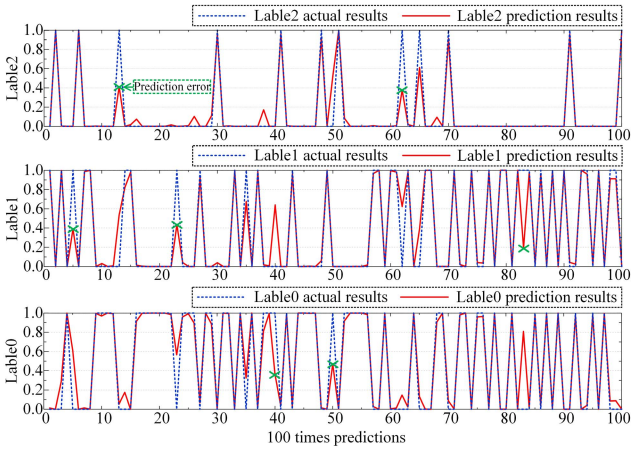

Fig. 14. Results of the 100 operations.

D. Performance Evaluation of the Human-Machine Collaborative Control Strategy

To evaluate the human-machine collaborative control strategy, eight experiments were performed in the experimental setup shown in Fig. 13. Each task was to insert the guidewire into the bifurcation within 120 s, in which the target point was set. Before the experiment, the operator tried ten exercises for knowing the insertion task. To verify the feasibility of the force-based perception method, the visual information was canceled. Only the human-machine interaction force and various kinds of information displayed on HMI were provided to the operator in the experiment. To test the effectiveness in different insertion states, different guidewire head shapes were set up. The human-machine collaborative control algorithm is shown in Alg. 1.

The results of the eight insertion experiments are shown in TABLE III. 58 decisions were made by the robot in the experiment. Among them, there were 54 consistent results of human-machine decision making, which showed that the operator had high trust in the prediction of the robot. Five of the eight experiments were successful, and the success rate was 62.5%. However, 50 correct operations conformed to the task

TABLE III
RESULTS OF THE EIGHT INSERTION EXPERIMENTS

Serial number	Decision making number	Decision making consistent number	Operator correct number	Maximum force			Success or not
				phase I (N)	phase II (N)	phase III (N)	
S1	10	8	10	3.32	3.36	3.80	S
S2	9	9	8	3.39	3.40	3.58	S
S3	7	7	5	3.54	3.53	3.82	F
S4	7	6	6	3.48	3.52	3.91	S
S5	7	7	6	3.42	3.53	3.71	S
S6	8	8	7	3.23	3.39	3.68	F
S7	6	5	4	3.36	3.32	3.38	F
S8	4	4	4	3.26	3.35	3.57	S

Algorithm 1 State Prediction and Collaborative Control Algorithm

Input: The optimized weight matrix $\mathbf{W}_{9\times3}$;
Output: The prediction results $P_r(t)$; The human-machine trust $T(t)$;
The master-slave collaborative mapping ratio $k(T(t))$;
1: For Timer on **do**
2: Input: the slave insertion position $x(t)$, the slave insertion force $F(t)$;
3: **If** Reach the end of the phase **Then**
4: The feature matrix in time t: ${x^t}_{1\times8}$;
5: Feature standardization;
6: Add the bias term: ${x^t}_{1\times9}$;
7: Substitution optimized model: $P_r(t) = \text{Softmax}\left({x^t}_{1\times9} \cdot \mathbf{W}_{9\times3}\right)$;
8: Transmitted to the HMI wirelessly;
9: **Endif**
10: Input the operation data: $\Delta\dot{x}(t)$, $\Delta\dot{x}(t-1)$, $T(t-1)$;
11: The human operation performance: $P_H(t)$;
12: The robot performance: $P_R(t)$;
13: The human-machine trust: $T(t) = T(t-1) + P_H(t) \cdot P_R(t) + E(t)$;
14: The master-slave collaborative mapping model: $k(T(t))$;
15: The multi-closed-loop PID control;
16: Delay until the timer interrupt is triggered;
17: End for

during the operation, and the correct rate was 86.21%, which met the expectation. The results showed the potentiality of the force-based perception method. All five obstructed states appeared in the phase III, and the model predicted success. In addition, the robot mistakenly predicted one entering the bifurcation state as obstructed state. TABLE III also showed that the maximum insertion force at phases I, II, and III gradually increased without obvious regularity.

Fig. 15 shows the position curve, the human-machine trust curve, and the master-slave mapping ratio curve of the experiment S1. The guidewire was inserted 10 times in three phases, where No. 0 and No. 1 belonged to phase I, No. 2 belonged to phase II, and No. 3 to No. 9 belonged to phase III. The robot

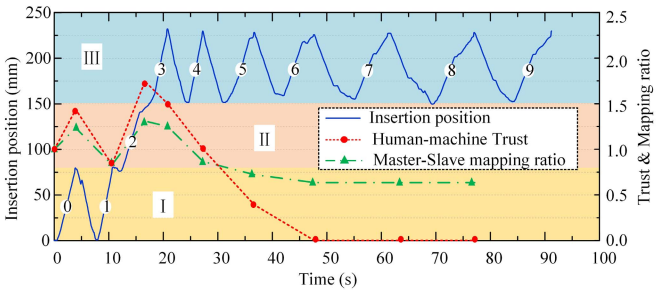

Fig. 15. Operation process of the experiment S1.

TABLE IV
PREDICTION RESULTS OF THE ROBOT

Number	Robot prediction results			Actual label	Operator decision making results
	Label 0	Label 1	Label 2		
0	0.001011	0.998965	0.000024	1	-1
1	0.385051	0.571418	0.043531	0	1
2	1	0	0	0	1
3	0.9978	0	0.0022	0	-1
4	0.969467	0.030532	0	0	-1
5	0.99999	0.000008	0.000002	0	-1
6	0.999591	0.000394	0.000015	0	-1
7	0.994007	0.005978	0.000014	0	-1
8	0.052574	0.537088	0.410338	2	-1
9	0.17607	0.823928	0.000002	1	1

Where operator decision making 1 represents inserting the guidewire continuously, -1 represents withdrawing the guidewire.

prediction results corresponding to each number are shown in TABLE IV.

1) Phase I: At the No. 0 insertion, the robot predicted that the guidewire entered the bifurcation closing to 100%. Based on the result and the perception of the interaction force, the operator considered that the guidewire entered the bifurcation and decided to withdraw the guidewire. The judgments of operator and robot were consistent. Combined the environmental factors, the human-machine trust was increased to 1.436616, and the master-slave mapping ratio was adjusted to 1.234175. At the No. 1, the robot reinserted the guidewire and predicted that the guidewire entered the bifurcation with a probability of 57.1418% and passed by the bifurcation with 38.5051%. The final label is label 1, but the operator considered that the guidewire passes by the bifurcation. The

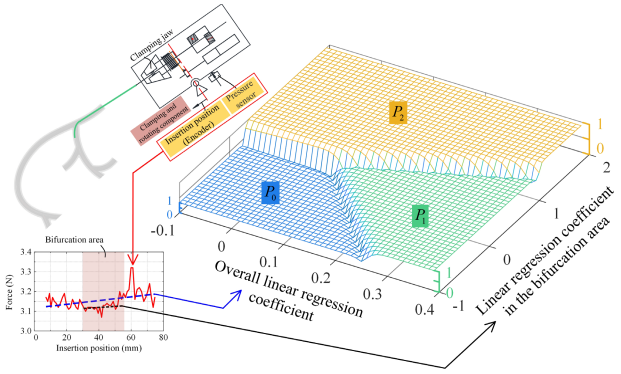

Fig. 16. Visualization of phase I prediction model.

judgments were inconsistent. To ensure safety, the trust was punished to 0.831775, and the master-slave mapping ratio was adjusted to 0.830029.

2) Phase II: At the No. 3, both the operator and the robot considered that the guidewire passed phase II smoothly. The trust was increased to 1.743663, and the master-slave mapping ratio was adjusted to 1.309738. The VIS robot was switched to the efficient operation mode.

3) Phase III: In this phase, entering the bifurcation was the expected path. Due to the small inner diameter of the vascular bifurcation, 7 insertions were performed. The situations of No. 3 to No. 7 were similar, in which the label 0 was close to 100%. Both the operator and the robot considered that the guidewire passed by the bifurcation. Although the human and robot judgments were consistent, the trust gradually decreased. The repeated insertion of the No. 3 to No. 6 decreased the trust from 1.743663 to 0 quickly. The master-slave mapping ratio was also decreased from 1.309738 to 0.634471 and the VIS robot was adjusted to the micro-operation mode. At the No. 3 insertion, the cumulative impact of environmental factors was greater than the impact of the consistent human-machine judgments, so the human-machine trust was decreased. In No. 8 insertion, the robot predicted that the guidewire entered the bifurcation. The operator considered that the guidewire passed by the bifurcation and withdrew. In No. 9 insertion, both the operator and the robot considered that the guidewire entered the bifurcation. The operator completed the insertion task, which took 91.2 s.

Overall, these experiments showed that the guidewire insertion state prediction model can predict the guidewire multi-states continuously in different environments. It indicates the feasibility and potentiality of the force-based perception method. The trust evaluation model evaluated the human-machine trust effectively based on the performance of the robot and the operator. Moreover, it automatically adjusted the master-slave mapping ratio to adapt to different surgical conditions.

To show the impact of robot force sensing on the prediction, the prediction model in phase I was visualized, as shown in Fig. 16. The overall linear regression coefficient and the linear regression coefficient in the bifurcation area were selected as the key features through principal component analysis (PCA). The two features were taken as the x-axis and y-axis respectively, and three labels probability were taken as the z-axis to draw a visualization of the prediction model. The rest of features were taken as the feature average and eliminated in the standardization. The results showed that the three labels were divided into three parts, as shown in the blue (label 0), green (label 1), and orange (label 2) grids in Fig. 16. These two key features focus on the variation of the insertion force with the position. Similarly, instead of only the size of the insertion force, surgeons focus on the change in guidewire insertion force with insertion depth to perceive insertion states, and this skill is implicit and empirical [20]. The proposed machine learning-based method explicitly expresses this skill, providing ideas for VIS robot force perception and force-based safety strategies.

IV. Discussion

The master-slave VIS robot system solves the problem of surgeons exposed to X-ray radiation in the operating room. Many researchers have paid attention to using the human-machine interaction force of the master manipulator to reproduce the weak insertion force of the slave robot. However, the difference between the master manipulator and the guidewire or catheter in morphology and physical parameters limits the contribution of force reproduction to the surgeons' judgments in surgery. Therefore, we used the slave robot, which collected surgical data lower delay and more directly, to predict the insertion state of the guidewire autonomously. Then the prediction results were transmitted to the master side to assist the surgeons' judgments. Meanwhile, we combined the robot prediction results with the operator's decision making to characterize the performance of human-machine collaboration and the complexity of the insertion environment, and adjust the master-slave mapping ratio dynamically for safety and efficiency. Zhao *et al.* [22] proposed a 1D CNN-based abnormal state recognizer, which performs the feasibility of the force-based prediction method. Compared with the recognizer, the insertion state prediction model can predict not only the abnormal insertion state but also whether the guidewire passed by or entered the bifurcation in the blood vessel model under the normal state. It better compensates for the inefficient acquisition of remote surgical force. We think that the following discussions are also necessary to enhance comprehension.

1) On the low success rate of collaboration control:

To verify the force-based perception method, we removed the influence of vision information though it is vital for operation. Moreover, the guidewire head shapes were set up unintentionally, which may not be able to complete the task. Therefore, a low success rate was obtained in the experiment. However, on the premise that the operator had high trust in the robot, the correct operation rate achieved 86.21%. The result verifies the effectiveness of the state prediction model. On the other hand, It is difficult for surgeons to complete the insertion task without the surgical image information and adjusting the guidewire head shape. In the future, the image data will be processed to enhance state perception.

2) On the sensing rate:

The sensing rate is vital for the real-time performance of the force-based perception method and also has an important influence on the data set collection. The basis program frame

was established on timer interrupt for ensuring the accurate refresh cycle. The maximum stable measurement rate of the master-slave system was 20 Hz considering the constraints of the communication delay between the MCU, sensors, and motor drivers.

3) On the difference of the maximum force of TABLE III: TABLE III showed that the minimum value of the maximum force was 3.38 N and the maximum value was 3.91 N in the phase III, which was a relatively large difference. The reason is that the obstructed state caused a large contact force between the guidewire and the blood vessel model. Besides, the different shapes of guidewire head also influenced contact force. Although the prediction model can predict the obstructed state, the insertion process was not suspended in time resulting in a relatively large contact force. Therefore, a robot-assisted system, which is not based on force measurement and has real-time force protection, may be designed in the future.

V. Conclusion

In this article, a novel VIS robot system was developed with the purposes of predicting guidewire insertion states and collaborative operating. To this aim, the weak guidewire insertion force was extracted and the human-machine interaction force was constructed. Meanwhile, a guidewire insertion state prediction model and a human-machine collaborative control strategy were proposed. Finally, a human-machine trust evaluation model and a master-slave collaborative mapping model were proposed, which can switch the master-slave operation mode to adapt to different surgical conditions. The experiment results demonstrated the feasibility and effectiveness of the force-based perception model and the collaborative strategy for enhancing the autonomy of the VIS robot.

Future studies will include the following: designing a robot-assisted system that is not based on force measurement and has real-time force insertion protection, enhancement of the performance to perceive the insertion state by adding more data about images.

References

[1] World Health Organization, "World health statistics 2021: Monitoring health for the SDGs, sustainable development goals," Geneva, Switzerland, Tech. Rep. 978-92-4-002705-3, May 2021. [Online]. Available: https://www.who.int/publications/i/item/9789240027053

[2] D. Wang, C. Yang, Y. Zhang, and J. Xiao, "Toward *in-vivo* force and motion measurement for vascular surgery," *IEEE Trans. Instrum. Meas.*, vol. 63, no. 8, pp. 1975–1982, Aug. 2014.

[3] A. Hooshiar, A. Payami, J. Dargahi, and S. Najarian, "Magnetostriction-based force feedback for robot-assisted cardiovascular surgery using smart magnetorheological elastomers," *Mech. Syst. Signal Process.*, vol. 161, Dec. 2021, Art. no. 107918.

[4] M. G. Andreassi, E. Piccaluga, G. Guagliumi, M. D. Greco, F. Gaita, and E. Picano, "Occupational health risks in cardiac catheterization laboratory workers," *Circulat., Cardiovascular Interventions*, vol. 9, no. 4, Apr. 2016, Art. no. e003273.

[5] L. W. Klein *et al.*, "Occupational health hazards of interventional cardiologists in the current decade: Results of the 2014 SCAI membership survey," *Catheterization Cardiovascular Interventions*, vol. 86, no. 5, pp. 913–924, Nov. 2015.

[6] L. W. Klein and E. P. Campos, "Occupational hazards in the cath lab—Physician, protect thyself!" *J. Invasive Cardiol.*, vol. 30, no. 2, pp. 75–76, 2018.

[7] X. Yin, S. Guo, N. Xiao, T. Tamiya, H. Hirata, and H. Ishihara, "Safety operation consciousness realization of a MR fluids-based novel haptic interface for teleoperated catheter minimally invasive neurosurgery," *IEEE/ASME Trans. Mechatronics*, vol. 21, no. 2, pp. 1043–1054, Apr. 2016.

[8] D. Kundrat *et al.*, "An MR-safe endovascular robotic platform: Design, control, and *ex-vivo* evaluation," *IEEE Trans. Biomed. Eng.*, vol. 68, no. 10, pp. 3110–3121, Oct. 2021.

[9] X. Yin, S. Guo, H. Hirata, and H. Ishihara, "Design and experimental evaluation of a teleoperated haptic robot–assisted catheter operating system," *J. Intell. Mater. Syst. Struct.*, vol. 27, no. 1, pp. 3–16, Nov. 2016.

[10] Z. Shaikh, M. Eilenberg, and T. Cohen, "The Amigo^{TM} remote catheter system: From concept to bedside," *J. Innov. Cardiac Rhythm Manage.*, vol. 8, no. 8, pp. 2795–2802, Aug. 2017.

[11] H. Shen, C. Wang, L. Xie, S. Zhou, L. Gu, and H. Xie, "A novel robotic system for vascular intervention: Principles, performances, and applications," *Int. J. Comput. Assist. Radiol. Surgery*, vol. 14, no. 4, pp. 671–683, Apr. 2019.

[12] X. Bao *et al.*, "Operation evaluation in-human of a novel remote-controlled vascular interventional robot," *Biomed. Microdevices*, vol. 20, no. 2, pp. 1–13, Jun. 2018.

[13] P. Kanagaratnam, M. Koa-Wing, D. T. Wallace, A. S. Goldenberg, N. S. Peters, and D. W. Davies, "Experience of robotic catheter ablation in humans using a novel remotely steerable catheter sheath," *J. Interventional Cardiac Electrophysiol.*, vol. 21, no. 1, pp. 19–26, Jan. 2008.

[14] Y. Kim, G. A. Parada, S. Liu, and X. Zhao, "Ferromagnetic soft continuum robots," *Sci. Robot.*, vol. 4, no. 33, pp. 1–32, Aug. 2019.

[15] S. Guo, Y. Wang, N. Xiao, Y. Li, and Y. Jiang, "Study on real-time force feedback for a master–slave interventional surgical robotic system," *Biomed. Microdevices*, vol. 20, no. 2, pp. 1–10, Jun. 2018.

[16] L. Zhang *et al.*, "Design and performance evaluation of collision protection-based safety operation for a haptic robot-assisted catheter operating system," *Biomed. Microdevices*, vol. 20, no. 2, pp. 1–14, Jun. 2018.

[17] X. Bao, S. Guo, N. Xiao, Y. Li, and L. Shi, "Compensatory force measurement and multimodal force feedback for remote-controlled vascular interventional robot," *Biomed. Microdevices*, vol. 20, no. 3, pp. 1–11, Sep. 2018.

[18] X. Jin, S. Guo, J. Guo, P. Shi, T. Tamiya, and H. Hirata, "Development of a tactile sensing robot-assisted system for vascular interventional surgery," *IEEE Sensors J.*, vol. 21, no. 10, pp. 12284–12294, May 2021.

[19] X. Jin *et al.*, "Total force analysis and safety enhancing for operating both guidewire and catheter in endovascular surgery," *IEEE Sensors J.*, vol. 21, no. 20, pp. 22499–22509, Oct. 2021.

[20] P. Shi *et al.*, "Design and evaluation of a haptic robot-assisted catheter operating system with collision protection function," *IEEE Sensors J.*, vol. 21, no. 18, pp. 20807–20816, Sep. 2021.

[21] X. Bao, S. Guo, N. Xiao, Y. Li, C. Yang, and Y. Jiang, "A cooperation of catheters and guidewires-based novel remote-controlled vascular interventional robot," *Biomed. Microdevices*, vol. 20, no. 1, pp. 1–19, Mar. 2018.

[22] Y. Zhao *et al.*, "A CNN-based prototype method of unstructured surgical state perception and navigation for an endovascular surgery robot," *Med. Biol. Eng. Comput.*, vol. 57, no. 9, pp. 1875–1887, 2019.

[23] S. Guo *et al.*, "Machine learning–based operation skills assessment with vascular difficulty index for vascular intervention surgery," *Med. Biol. Eng. Comput.*, vol. 58, no. 8, pp. 1707–1721, Aug. 2020.

[24] Y. Zhao *et al.*, "A novel noncontact detection method of surgeon's operation for a master-slave endovascular surgery robot," *Med. Biol. Eng. Comput.*, vol. 58, no. 4, pp. 871–885, Apr. 2020.

[25] S. Guo, Y. Song, and X. Yin, "A novel robot-assisted endovascular catheterization system with haptic force feedback," *IEEE Trans. Robot.*, vol. 35, no. 3, pp. 685–696, Mar. 2019.

[26] J. Guo, S. Guo, L. Shao, P. Wang, and Q. Gao, "Design and performance evaluation of a novel robotic catheter system for vascular interventional surgery," *Microsyst. Technol.*, vol. 22, no. 9, pp. 2167–2176, Sep. 2016.

[27] W. Chi, J. Liu, H. Rafii, C. Riga, C. Bicknell, and G. Yang, "Learning-based endovascular navigation through the use of non-rigid registration for collaborative robotic catheterization," *Int. J. Comput. Assist. Radiol. Surg.*, vol. 13, no. 6, pp. 855–864, Jan. 2018.

[28] Y. Song *et al.*, "Performance evaluation of a robot-assisted catheter operating system with haptic feedback," *Biomed. Microdevices*, vol. 20, no. 2, pp. 1–16, Jun. 2018.

[29] T. Haesevoets, D. De Cremer, K. Dierckx, and A. Van Hiel, "Human-machine collaboration in managerial decision making," *Comput. Hum. Behav.*, vol. 119, Jun. 2021, Art. no. 106730.

[30] A. Stevenson, A. Kirresh, M. Ahmad, and L. Candilio, "Robotic-assisted PCI: The future of coronary intervention?" *Cardiovascular Revascularization Med.*, vol. 35, pp. 161–168, Feb. 2022.
[31] N. Moray, T. Inagaki, and M. Itoh, "Adaptive automation, trust, and self-confidence in fault management of time-critical tasks," *J. Experim. Psychol., Appl.*, vol. 6, no. 1, pp. 44–58, 2000.
[32] Y. Zhao, "Study on experience-learning-based human-machine collaborative strategy for an endovascular surgery robot," Ph.D. dissertation, Dept. Biomed. Eng., Beijing Inst. Technol., Beijing, China, 2019.

Yonggan Yan (Graduate Student Member, IEEE) received the B.S. degree in mechanical design manufacturing and automation and the M.S. degree in mechanical engineering from Yanshan University, Hebei, China, in 2018 and 2021, respectively. He is currently pursuing the Ph.D. degree with the Beijing Institute of Technology, Beijing, China.

He has published three refereed journal articles and conference papers. He researches on master–slave systems for remote surgical robots, and biomedical applications of surgical robots.

Hongbo Wang (Member, IEEE) received the B.S. and M.S. degrees from the Northeast Heavy Machinery Institute, Qiqihar, China, in 1982 and 1986, respectively, and the Ph.D. degree from Nagasaki University, Nagasaki, Japan, in 1997.

He studied as a Visiting Scholar at the Institute of Robotics, ETH Zürich, Switzerland, from 1992 to 1993. After that, he moved to Nagasaki University as a Researcher. In 1998, he worked with DAIHEN Corporation, Osaka, Japan, as the Deputy Manager. In 2009, he worked with Yanshan University, Qinhuangdao, China, as a Professor. Since 2021, he has been working with Fudan University, Shanghai, China, as a Professor. He has published about 160 papers in journals and international conferences. He has presided over and participated in a number of national projects including the National Natural Science Foundation of China. His current research interests are in parallel robot, surgery robot, rehabilitation robot, and assisting robot for the disabled and the elderly.

Haoyang Yu received the B.S. degree in mechanical and electrical engineering from Hainan University, Hainan, China, in 2012. He is currently pursuing the M.S. and Ph.D. degrees with Yanshan University, Hebei, China.

His research interests include master–slave systems for remote surgical robots, force perception of surgical robots, and clinical applications of surgical robots.

Fuhao Wang (Graduate Student Member, IEEE) received the B.S. degree in mechanical design and manufacturing and automation from the East China University of Science and Technology, China, in 2018. He is currently pursuing the Ph.D. degree with Fudan University, majoring in biomedical engineering.

At present, he mainly researches medical robots, especially the modeling and control of flexible surgical robots.

Junyu Fang received the B.S. degree in mechanical engineering from the China University of Mining and Technology, Jiangsu, China, in 2018. He is currently pursuing the M.S. degree with Yanshan University, Hebei, China.

His research direction is in master–slave systems for remote surgical robots.

Jianye Niu received the B.S. degree in mechanical engineering and the M.S. and Ph.D. degrees in mechatronic engineering from Yanshan University, Qinhuangdao, Hebei, China, in 2005, 2008, and 2019, respectively.

He is currently an Associate Professor with the School of Mechanical Engineering, Yanshan University. His research interests include parallel mechanism and its application, rehabilitation robot, mechanical engineering, and artificial neural networks.

Shuxiang Guo (Fellow, IEEE) received the Ph.D. degree in mechano-informatics and systems from Nagoya University, Japan, in 1995.

He is currently a Full Professor with the Faculty of Engineering and Design, Kagawa University, Takamatsu, Japan. He is also the Chair Professor with the Key Laboratory of Convergence Medical Engineering System and Healthcare Technology, Ministry of Industry and Information Technology, Beijing Institute of Technology, Beijing, China. He has published about 500 refereed journals and conference papers. His current research interests include biomimetic underwater robots, medical robot systems for minimal invasive surgery, micro catheter systems, micropump, and smart material (SMA and IPMC) based on actuators.

Prof. Guo is the Editor-in-Chief of the *International Journal of Mechatronics and Automation*.